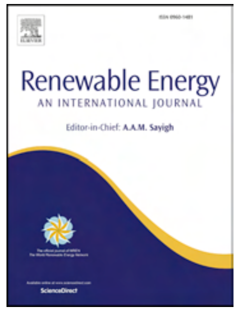

Mooring-based frequency-domain and AI-based time-domain optimization for improved power capture performance of the TALOS wave energy converter

Hakan YAVUZ, Wanan SHENG, George AGGIDIS

PII: S0960-1481(26)00066-2

DOI: https://doi.org/10.1016/j.renene.2026.125241

Reference: RENE 125241

To appear in: *Renewable Energy*

Received Date: 3 August 2024

Revised Date: 28 December 2025

Accepted Date: 8 January 2026

Mooring-based frequency-domain and AI-based time-domain optimization for improved power capture performance of the TALOS wave energy converter

Hakan YAVUZ[a], Wanan SHENG[b], George AGGIDIS[c]

[a]Cukurova University, Faculty of Engineering, Dept. of Mech. Eng., Saricam, Adana, TURKIYE. hyavuz@cu.edu.tr, dr.hakanyavuz@gmail.com

[b]Department of Aerospace and Mechanics, South-East Technological University (SETU), Ireland. wanan.sheng@setu.ie

[c]Lancaster University, School of Engineering, Gillow Ave, Bailrigg, Lancaster LA1 4YW, UK g.aggidis@lancaster.ac.uk

Corresponding author:

Hakan YAVUZ, Cukurova University, Faculty of Engineering, Dept. of Mech. Eng., Saricam, Adana, TURKIYE. hyavuz@cu.edu.tr , dr.hakanyavuz@gmail.com

Mooring-based frequency-domain and AI-based time-domain optimization for improved power capture performance of the TALOS wave energy converter

Abstract:

Mooring-based frequency-domain analysis combined with AI-based time-domain optimization offers a systematic approach to improving power capture performance in multi-degree-of-freedom wave energy converters. While most existing studies focus on single-degree-of-freedom systems, enhanced energy absorption can be achieved by exploiting the dynamic potential of multi-DoF configurations. This study investigates the TALOS wave energy converter, a six-degree-of-freedom system, with the objective of improving its power capture capability through coordinated mooring and power take-off (PTO) optimization. The optimization framework begins with a frequency-domain analysis to assess the influence of mooring parameters on the system response. Based on this analysis, two refined configurations, denoted as TALOS-L and TALOS-H, are developed using optimized mooring stiffness characteristics. Subsequently, time-domain simulations are conducted using a genetic algorithm to determine optimal PTO damping settings under site-specific sea conditions. The results show that adaptive tuning of both mooring and PTO parameters significantly improves power capture across different sea states. In particular, the TALOS-H configuration, featuring tuned surge mooring stiffness and genetically optimized PTO damping, consistently outperforms the baseline configuration. These findings highlight the importance of site-specific tuning and demonstrate the effectiveness of AI-based optimization for enhancing the adaptability and efficiency of multi-degree-of-freedom wave energy converters.

Keywords: TALOS wave energy converter; multi-DoF system modeling; frequency-domain mooring analysis; time-domain optimization; PTO damping optimization; genetic algorithm.

1. Introduction

Interest in renewable energy systems has increased in response to recurring fossil fuel–based energy crises and associated economic challenges. In recent decades, these issues have become more pronounced, alongside growing concern over climate change and its environmental impacts. As a result, the development of environmentally sustainable energy technologies has become an important research priority. Within this context, renewable energy systems capable of contributing to long-term energy security and environmental protection are receiving increasing attention.

Some renewable energy systems, such as wind and solar energy, have reached high level of technological maturity with a considerable level of installed capacity worldwide. Hence, the next target is to advance wave energy to comparable levels of development. This is critical to ensure that wave energy systems are also utilized to a considerable extent, thereby, achieving almost the full utilization of environmentally friendly renewable sources. It is worth noting that wave energy is actually a concentrated form of wind energy generated by solar radiation absorbed by the oceans and seas. The global wave energy resource has been evaluated from regional, global, and nearshore perspectives. Regional offshore assessments report high extractable wave energy levels in countries such as the UK, Brazil, and New Zealand [1], global-scale analyses highlight the large yet underexploited potential of wave power and its applicability in regions with declining hydropower availability [2] and nearshore resource studies estimate a technically exploitable capacity of 100–800 TWh yr^{-1} worldwide [3]. In addition, global assessments indicate that the total wave energy potential is substantial, with estimates ranging from 17,500 [4] to 26,000 TWh [5] and from 8,000 to 80,000 TWh depending on assessment methodology and assumptions [6].

Considering the attractive energy potential, it is not surprising that many wave energy converter models have been suggested and patented over last century. The early patented models even date back to the early 19th century. Similarly, as a research field, the topic attracts the attention of many researchers and thousands of studies have been reported in the literature so far. Despite all these efforts, very few of these wave energy converter designs have progressed to full-scale sea deployment and survived the harshness of the seas.

Generally, the most powerful waves are encountered in deep-water regions, often far out at sea and in the oceans. The waves in deep waters naturally have greater energy content than those in shallower waters near land [7]. Hence, offshore devices are expected to exhibit higher energy capture potential relative to nearshore or onshore systems. However, offshore devices are far more difficult to construct and maintain than onshore or nearshore devices due to the same energetic wave conditions that can potentially cause structural damage to the wave energy converter systems.

Many studies in the wave energy literature are limited to single-degree-of-freedom (SDOF) systems, predominantly heaving buoys. Eidsmoen [8] and Korde [9] investigated single-DoF heaving devices, focusing on phase control and reaction force mechanisms, respectively. Single-DoF latching control strategies were examined by Korde [10] and extended to reactively loaded oscillating bodies by Korde [11]. Babarit et al. [12] and Nolan et al. [13] studied single-DoF heaving systems with emphasis on latching strategy comparison and PTO modeling. Experimental and theoretical analyses of single-DoF heaving converters were reported by Bjarte-Larsson and Falnes [14] and Shi et al. [15]. Optimization-oriented studies also predominantly adopted a single-DoF assumption, including geometric optimization of heaving point absorbers [16] and spectral-domain PTO sizing for heave motion [17]. More recent works optimized single-DoF heaving systems using model predictive control [18] and high-fidelity SPH-based numerical simulations [19]. Hillis et al. [20] also highlighted the dominance of single-DoF heaving systems in the literature and noted the comparatively limited attention given to the development and control of multi-DoF WEC systems.

As reported by Yavuz [21], one of the main reasons for the popularity of single-DoF systems is that an increasing number of degrees of freedom (DoF) in a wave energy converter (WEC) not only leads to complexities in its behavior but also makes understanding the WEC's interaction with the sea a challenging technical issue. Consequently, higher system complexity makes WECs more difficult to understand, model and simulate. In their study of a multi-DoF wave energy converter system, Hillis et al. [20] reported that they aimed not only to develop an active control strategy to maximize power capture but also to limit device loading to prolong its lifespan. Additionally, they preferred to use only physically measurable quantities in the controller design, thereby focusing on the development of a realistic, deployable system.

Abdelkhalik et al. [22] studied the control of a three-DoF floating point absorber based on heave, surge, and pitch modes of motion. Their work focused on optimizing the pitch and surge modes where various control strategies were applied and the corresponding results reported.

Galvan-Pozos and Ocampo-Torres [23] reported a novel six-DoF WEC design based on the Stewart-Gough platform, aimed at establishing the necessary equations to describe the motion of the platform. Using linear wave theory, the instantaneous and mean power were calculated under regular wave conditions. The reported results indicate that the proposed configuration could increase wave energy conversion, since all degrees of freedom in its motion were utilized, compared to traditional heaving point absorber WEC systems.

There are many wave energy converter models that have been considered for development. Amongst them, as mentioned earlier, offshore types appear to have the highest energy capture potential, and oscillating types seem to be among the most popular [7]. The Bristol cylinder is an example of a multi-DoF wave energy converter system. It is a cylindrical device that extracts power from heave, surge, and pitch motion modes [24]. There have been some more recent studies on this converter system focusing on its control [25], mainly on power electronic hardware rather than active control strategies. Additionally, Crowley et al. [26] reported alternative arrangements that enhanced the practicality of the power-capturing functionality.

The modeling of Wave Energy Converters (WECs) is a highly complex task, particularly for multi-degree-of-freedom (multi-DoF) systems, where dynamic interactions between motion modes significantly increase complexity. Extensive research exists on WEC modeling, design, analysis, and control strategies, with studies ranging from simpler single-degree-of-freedom (1-DoF) systems to more complex multi-DoF configurations. While single-DoF

WECs allow for more straightforward control and optimization, multi-DoF systems present greater challenges due to nonlinear interactions, mooring effects, and site-specific dynamics.

One often overlooked aspect in WEC modeling is the influence of mooring configurations on the system's dynamic response. Mooring not only affects stability but also plays a crucial role in shaping the system's response amplitude operators (RAOs), thereby influencing energy capture efficiency. Additionally, the inherent coupling effects between different motion modes make it difficult to predict and optimize system behavior. Another key challenge in WEC design is the need for site-specific adaptation, which is part of standard practice and ensures that the device's resonance characteristics align with the dominant wave conditions of the deployment location. The integration of an advanced multi-DoF Power Take-Off (PTO) model further complicates the design process, requiring a careful tuning of PTO settings to accommodate varying sea states while maximizing power conversion efficiency.

In this study, a systematic design and optimization approach for a multi-DoF WEC is proposed and applied to the TALOS wave energy converter. The study builds upon two existing WEC configurations—a hard-moored and a soft-moored variant—previously reported in the literature. A comprehensive frequency-domain and time-domain analysis is conducted for a selected deployment site to assess the effects of mooring configurations on dynamic performance. To enhance energy capture efficiency, a multi-objective optimization framework is introduced for tuning the 6-DoF PTO system, leveraging a Genetic Algorithm (GA) for optimal damping settings. The findings demonstrate that mooring configurations significantly influence the WEC's dynamic behavior, offering a mechanism to tailor the system's RAO characteristics and shift resonance frequencies toward the dominant wave conditions of the deployment site. This, in turn, facilitates a more manageable and effective tuning of PTO parameters. The results also indicate that, despite the system's complexity, surge, heave, and pitch motions remain the dominant modes influencing energy capture, and therefore constitute the primary focus of the optimization process.

By addressing these challenges, this study contributes to the growing body of research on multi-DoF WEC modeling, mooring-integrated system optimization, and AI-based PTO tuning techniques. The findings offer additional insights into the role of mooring in dynamic tuning, reinforcing the necessity of site-specific adaptations for efficient WEC operation.

The TALOS WEC is a recently developed multi-degree-of-freedom wave energy converter, designed by a research team at Lancaster University. It is a six-degree-of-freedom (6-DoF) device that captures wave energy from all available motion modes, distinguishing it from conventional single-axis WECs. This innovative approach presents both opportunities and challenges, as the increased number of degrees of freedom introduces complex coupling effects that must be carefully analyzed and optimized.

Several studies have explored key aspects of TALOS WEC's performance and control strategies. Aggidis and Taylor [27] provided a foundational overview of single-axis and multi-axis WEC technologies, introducing the first tank-tested model of TALOS. Subsequent research by Sheng et al. [28] examined the hydrodynamic behavior of the device, while Hall et al. [29] investigated model predictive control strategies for optimizing its performance. Additional contributions by Sheng and Aggidis [30], Michailides et al. [31], and Yavuz et al. [32] have further refined our understanding of the hydrodynamics, time-domain simulations, and power capture performance of the TALOS system using complementary computational tools. However, despite these advancements, critical aspects of mooring dynamics and PTO optimization in irregular waves remain underexplored, particularly in the context of site-specific deployment challenges.

The primary objective of this study is to advance understanding and optimization of the TALOS WEC's power capture performance by addressing key challenges in mooring dynamics, frequency-domain response, and power take-off (PTO) optimization. Specifically, the study aims to:

- Investigate the role of mooring configurations in shaping the dynamic response of the TALOS WEC, particularly in shifting its response amplitude operators (RAOs) to align with dominant wave frequencies at a selected deployment site.
- Evaluate system performance in both frequency and time domains to provide a comprehensive analysis of its behavior under realistic sea conditions.
- Optimize the multi-DoF PTO system using a Genetic Algorithm (GA), ensuring that damping settings are tuned for maximum power absorption while considering site-specific variations in wave conditions.
- Demonstrate the importance of site-specific tuning, showing that optimizing the mooring and PTO settings together significantly enhances energy extraction efficiency.
- Provide new insights into the complex interactions between motion modes in multi-DoF WECs, reinforcing the need for integrated modeling, control, and optimization frameworks in wave energy research.

By integrating mooring design, hydrodynamic analysis, and AI-based optimization, this study addresses a critical gap in existing TALOS WEC research and contributes to the broader field of multi-DoF WEC modeling and control strategies. The findings are expected to offer valuable guidelines for future WEC designs and site-specific adaptation methodologies, thereby advancing the state-of-the-art in wave energy conversion technology.

This study begins with an introduction to the physical system model, providing an overview of the TALOS wave energy converter and its key components. It then presents the mathematical modeling framework, starting with the frequency-domain model, followed by a detailed analysis of the TALOS system in the frequency domain. The time-domain model is then developed to extend the analysis for dynamic system evaluation. Next, the power capture properties of the moored TALOS system are assessed using both frequency and time-domain analyses. The study further investigates the power capture performance of the optimized system, incorporating tuning strategies to enhance energy extraction. Finally, the work concludes with a summary of key findings.

2. The Physical System Model

In this study, an offshore oscillating-type wave energy converter (WEC) system is selected for analysis. The following sections provide a detailed overview of the modeling and control application of the WEC. The physical configuration of the 6-DoF TALOS WEC, developed by the Lancaster University Wave Energy Group, is illustrated in Fig. 1. This multi-degree-of-freedom device is represented in meshed form (Fig. 1a), a rendered image (Fig. 1b), and its original power take-off (PTO) system (Fig. 1c) in the figure. The key physical properties of the TALOS WEC used in this study are summarized in Table 1 [30, 31].

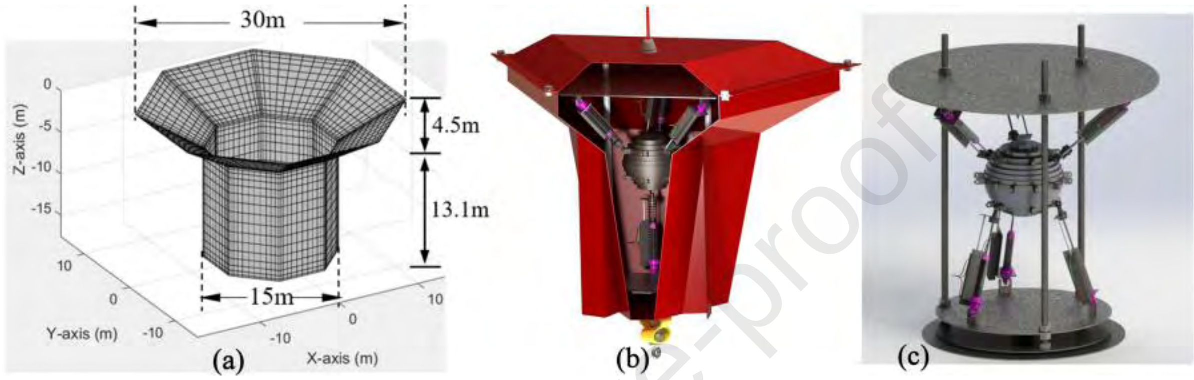

Fig. 1. The TALOS WEC, developed by Lancaster University Wave Energy Group. **a)** TALOS I: shape and panels, **b)** TALOS II with PTO system, **c)** TALOS PTO test rig

Table 1. Physical properties of the TALOS WEC

Par	Description	Value	Unit
D_c	diameter	D_1=15, D_2=30	m
-	Draft	17.60	m
V_d	displaced volume of water	3754.75	m^3
m_{dry}	inertial mass	3048.6	tonne
m_b	spherical PTO ball mass	800	tonne
CoG	dry centre of gravity	-7.96	m
Co	Center of buoyancy	-6.92	m
C_{11}	Mooring lines equivalent stiffness in surge (K_{11})	5E05 (**Soft moored,** [31]) 2.50E08 (**Hard moored,** [30])	N/m
C_{22}	Mooring lines equivalent stiffness in sway (K_{22})	5E05 (**Soft moored,** [31]) 2.50E08 (**Hard moored,** [30])	N/m
C_{33}	Restoring coefficient in heave	6.397E06	N/m
C_{44} C_{55}	Restoring coefficients in roll/pitch	3.636E08	N/rad

***C*₆₆**	Mooring lines equivalent stiffness in yaw *(K_{66})*	2.5E06 (**Soft moored,** [31]) 5.00E08 (**Hard moored,** [30])	N/rad
$\boldsymbol{I_{xx}}$	Moment of inertia	2.376E08	kg.m^2
$\boldsymbol{I_{yy}}$	Moment of inertia	2.376E08	kg.m^2
$\boldsymbol{I_{zz}}$	Moment of inertia	2.448E08	kg.m^2

Table 1 presents the physical properties of the TALOS WEC, including key mooring parameters (C_{11}, C_{22}, C_{66}) provided for two different mooring configurations of the model. The mooring settings reported by Michailides et al. [31] are relatively lower in stiffness compared to those presented by Sheng and Aggidis [30]. To distinguish between these variations, the two configurations are labeled as soft-moored [31] and hard-moored [30].

3. The Mathematical Model

Frequency domain (FD) analysis is a key step in the design process of wave energy converter (WEC) systems. Its primary objectives include the identification and tuning of WEC parameters, mooring configurations, and power take-off (PTO) system properties, as well as performing preliminary performance evaluations of the device.

Since frequency domain analysis is inherently linear, it cannot account for significant nonlinear effects that arise under high and extreme sea conditions, as noted by Eidsmoen [8]. Therefore, the results must be interpreted within the context of these limitations. While more comprehensive assessments can be conducted through time-domain simulations, frequency domain analysis remains a valuable tool for early-stage design evaluation, helping to identify resonance frequencies, general frequency response characteristics, and initial estimates of power capture capacity.

Developing an accurate WEC model requires consideration of several interrelated factors. In the frequency domain, key parameters such as Response Amplitude Operators (RAOs), Froude-Krylov forces, diffraction and radiation effects, and added mass properties play a crucial role in the dynamic assessment of the system. Taking these aspects into account, the following section presents the FD formulation of the TALOS WEC used in this study.

3.1. Frequency-Domain Model

The frequency-domain dynamic equation of 6-degrees of freedom (DoFs) motions of a rigid structure is given in a form of mass-spring-damper system [33], as

$$\sum_{k=1}^{6}\left\{-\omega^2\left[M_{jk}+M_{ij}^{E}+A_{jk}(\omega)\right]+i\omega\left[B_{jk}(\omega)+B_{jk}^{E}\right]+\left(C_{jk}+C_{jk}^{E}\right)\right\}\xi_k(\omega)=F_j(\omega) \quad (1)$$

where

ω is the circular frequency of the wave excitation, and the parameters with the variable ω mean their frequency dependency;

$M_{jk}, M_{jk}^{E}, A_{jk}(\omega)$ $(j, k = 1, 2, \dots, 6)$ are the structure, external and added mass matrices, and the first two must be specified for the numerical modelling, while the last can be assessed using the panel method;

$B_{jk}(\omega), B_{jk}^{E}$ $(j, k = 1, 2, \dots, 6)$ are the radiation and external damping coefficients, with the first being assessed using the panel method, while the last must be specified in the numerical modeling;

C_{jk}, C_{jk}^{E} $(j, k = 1, 2, \dots, 6)$ are the structure hydrostatic and external restoring coefficients (both must be specified or calculated). The definition of the hydrostatic restoring coefficients C_{jk} can be found in WAMIT manual [33];

$F_j(\omega)(j = 1, 2, \dots, 6)$ are the frequency-dependent complex amplitude of the wave excitation, which can be calculated using the panel method;

$\xi_k(\omega)(k = 1, 2, \dots, 6,$ correspond to the motions of surge, sway, heave, roll, pitch, and yaw, respectively. These represent the frequency-dependent complex amplitudes of motion of the floating structure, which are obtained by solving the dynamic equation above. In practical applications, a more useful representation is the Response Amplitude Operator (RAO), defined as:

$$\chi_k = \frac{\xi_k}{A} \qquad (2)$$

where *A* is the wave amplitude (here the wave amplitude *A* is without a subscript or superscript).

Obviously in the wave of a unit amplitude, the frequency-dependent ξ_k itself is the RAO. In the conventional plots, the module of the RAO may be more often seen, which is calculated as

$$|\chi_k| = \frac{|\xi_k|}{A} \qquad (3)$$

From the terms related to the added mass, radiation damping, and restoring coefficients in Eq. (1), the motions of a free-floating structure may become coupled through the cross-coupling coefficients. The motion couplings can occur through the wave radiation, which is caused by the cross-coupling of added mass and radiation damping coefficients. For instance, if the coupling coefficients such as A_{15} (surge-pitch coupling) or B_{24} (sway-roll coupling) are not zero or are significantly larger than other terms, such as A_{11} and B_{22}, the motions will be coupled. Additionally, motion couplings can arise from the hydrostatic restoring coefficients. For example, the coupling between heave and roll (or pitch), represented by coefficients like C_{34} or C_{35}, also contributes to the overall motion coupling.

It should be noted that some of the coupled motions are inherently present, such as surge-pitch coupling and sway-roll coupling, while others may or may not exist, depending on the shape and geometry of the floating structure. For example, the symmetry of the structure about the x-axis could cause the C_{35} coefficient to be zero, effectively decoupling heave and pitch in terms of the restoring coefficient.

3.2. Frequency-Domain Analysis of the TALOS Model

The frequency-domain model of the TALOS system is evaluated based on its initial design parameters [30,31]. Response Amplitude Operators (RAOs), a type of transfer function, are used to quantify the effect of a sea state on the structure in regular seas for a unit wave height at a specific frequency. This approach allows identification of frequencies that produce maximum motion amplitudes and, consequently, maximum power capture. Using Eq. 3, the RAOs for the different motion modes of the initial system model can then be calculated.

The targeted sea site has been selected as the EMEC site, as reported by Babarit et al. [34]. In their study, they presented detailed information on the peak period (T_p) and significant wave height (H_s) of the site, which is shown as a scatter diagram.

Table 2. Scatter diagram for the EMEC site [34]

$H_s(m)/T_p(s)$	5.00	6.55	8.11	9.66	11.22	12.77	14.33	15.88	17.44	19.00
10.00	0	0	0	0	0	0	0	0	0	1
9.50	0	0	0	0	0	0	0	0	1	1
9.00	0	0	0	0	0	0	0	1	2	1
8.50	0	0	0	0	0	0	0	1	2	1
8.00	0	0	0	0	0	0	1	4	4	1
7.50	0	0	0	0	0	0	2	7	5	0
7.00	0	0	0	0	0	0	5	9	4	0
6.50	0	0	0	1	1	2	9	10	2	0
6.00	0	0	0	1	1	7	18	11	1	0
5.50	0	0	0	1	18	26	15	7	0	0
5.00	0	0	0	11	46	42	7	2	1	0
4.50	0	0	1	49	78	36	6	2	1	0
4.00	0	0	17	114	119	25	5	2	1	0
3.50	0	3	91	191	118	19	5	2	1	0
3.00	1	29	211	252	80	16	7	3	1	0
2.50	7	151	339	244	61	19	10	3	1	0
2.00	54	338	433	193	61	22	9	2	0	0
1.50	200	508	448	174	62	20	7	1	0	0
1.00	408	629	391	151	52	15	6	2	0	0
0.50	393	455	233	87	33	14	6	2	0	0

The details listed in Table 2 [34] provide the most likely wave conditions (highlighted in red) that are critical for the development of the TALOS WEC to maximize its power capture performance. Wave conditions with $H_s > 5\,m$ or $T_p > 12\,s$ represent relatively rare sea states, accounting for only ~6.3 % of all recorded occurrences. Therefore, the TALOS WEC is optimized for sea conditions corresponding to $0 < H_s \leq 5\,m$ and $5\,s \leq T_p \leq 12\,s$. To optimize the system properties, four main sea states have been identified, characterized by H_s values of

1, 2, 3, and 4 meters, and T_p values of 6, 7, 8, and 9 seconds. These sea states define the operational range for testing the TALOS WEC system.

3.3. Time Domain Model of TALOS

The mathematical models of floating-body type WECs are often expressed in the frequency domain. These models characterize the system's response to the frequency content of the waves, making them particularly useful for analyzing steady-state responses under dominant wave components, although they can also be applied to irregular seas using spectral discretization. However, in real-world conditions, the motion of the free surface rarely attains steady-state behavior, making a time-domain (TD) representation more suitable. In such cases, the dynamic equations that define the motion of a free-floating body are formulated in the time domain (TD). Along with the usual instantaneous forces (which are proportional to the acceleration, velocity, and displacement of the body), the most commonly used formulations of the time-domain model of a floating body include convolution integral terms [35] to account for the memory effects of wave radiation on the free surface. As for wave force computation, this process becomes non-causal, requiring knowledge of the future wave elevation history [36].

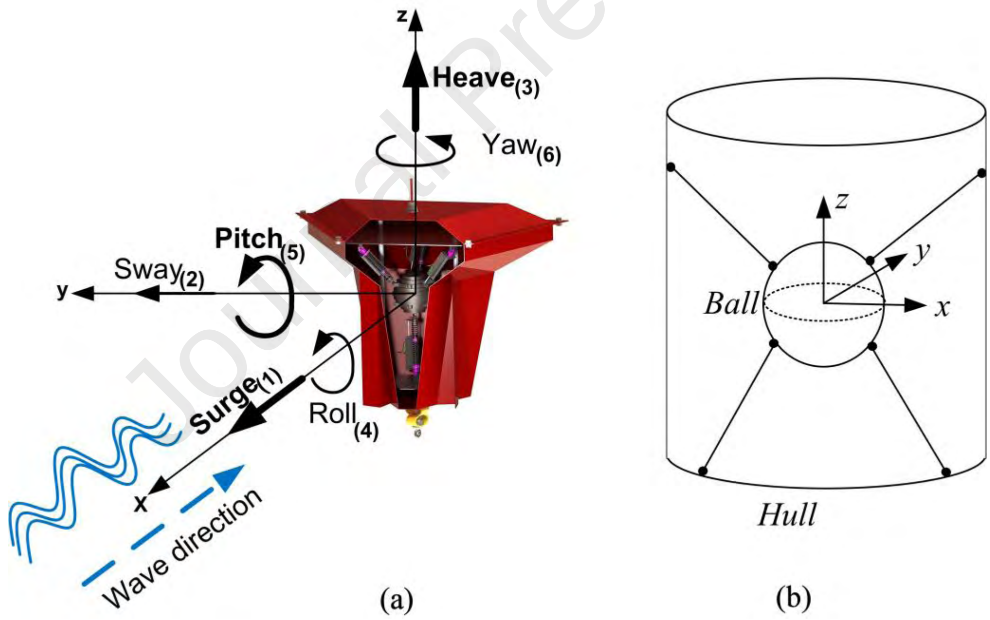

Fig. 2. The TALOS WEC: **(a)** Inner structure and corresponding body motions, **(b)** Rigid connections between the hull and the ball.

The TALOS WEC is excited by both regular and irregular waves, which generate wave forces on the device hull. Given that the TALOS WEC is a six-degree-of-freedom (6-DoF) device, all six body motions (Fig. 2a) are considered in the time-domain (TD) model of the system. The spherical ball-shaped mass (Fig. 2b) responds to these motions, generating relative motion across the six DoFs. This relative motion is then converted into captured power using the installed power take-off (PTO) unit. Since the PTO system is also a 6 DoF type, all motion modes contribute to the captured power. The layout of the inner structure and detailed mechanisms are shown in Fig. 1(c), and a schematic diagram is provided in Fig. 2b.

To perform the necessary simulations, the time-domain (TD) model of the TALOS WEC is developed. The following set of equations defines the motion for the six degrees of freedom (DoF) motion modes: surge, sway, heave, roll, pitch, and yaw (denoted from 1 to 6, respectively) of the TALOS WEC.

$$\begin{cases} m_s\ddot{x}_{h1}(t) + \sum_{j=1}^{6} A_{1j}\,\ddot{x}_{hj}(t) + \sum_{j=1}^{6}\int_0^t K_{1j}(t-\tau)\dot{x}_{hj}(\tau)d\tau + \sum_{j=1}^{6} C_{1j}\,x_{hj}(t) = F_1^{ex}(t) - F_{h1}^{pto}(t) - F_{h1}^{spr}(t) \\ m_s\ddot{x}_{h2}(t) + \sum_{j=1}^{6} A_{2j}\,\ddot{x}_{hj}(t) + \sum_{j=1}^{6}\int_0^t K_{2j}(t-\tau)\dot{x}_{hj}(\tau)d\tau + \sum_{j=1}^{6} C_{2j}\,x_{hj}(t) = F_2^{ex}(t) - F_{h2}^{pto}(t) - F_{h2}^{spr}(t) \\ m_s\ddot{x}_{h3}(t) + \sum_{j=1}^{6} A_{3j}\,\ddot{x}_{hj}(t) + \sum_{j=1}^{6}\int_0^t K_{3j}(t-\tau)\dot{x}_{hj}(\tau)d\tau + \sum_{j=1}^{6} C_{3j}\,x_{hj}(t) = F_3^{ex}(t) - F_{h3}^{pto}(t) - F_{h3}^{spr}(t) \\ I_{s44}\ddot{x}_{h4}(t) + \sum_{j=1}^{6} A_{4j}\,\ddot{x}_{hj}(t) + \sum_{j=1}^{6}\int_0^t K_{4j}(t-\tau)\dot{x}_{hj}(\tau)d\tau + \sum_{j=1}^{6} C_{4j}\,x_{hj}(t) = F_4^{exc}(t) - M_{h1}^{pto}(t) - M_{h1}^{spr}(t) \\ I_{s55}\ddot{x}_{h5}(t) + \sum_{j=1}^{6} A_{5j}\,\ddot{x}_{hj}(t) + \sum_{j=1}^{6}\int_0^t K_{5j}(t-\tau)\dot{x}_{hj}(\tau)d\tau + \sum_{j=1}^{6} C_{5j}\,x_{hj}(t) = F_5^{ex}(t) - M_{h2}^{pto}(t) - M_{h2}^{spr}(t) \\ I_{s66}\ddot{x}_{h6}(t) + \sum_{j=1}^{6} A_{6j}\,\ddot{x}_{hj}(t) + \sum_{j=1}^{6}\int_0^t K_{6j}(t-\tau)\dot{x}_{hj}(\tau)d\tau + \sum_{j=1}^{6} C_{6j}\,x_{hj}(t) = F_6^{ex}(t) - M_{h3}^{pto}(t) - M_{h3}^{spr}(t) \end{cases} \quad (4)$$

where

x_{hk} (k = 1, 2, …, 6) are the structure motions, representing the six degrees of freedom (DoFs) of the hull, which will be solved from the dynamic equation.

A_{jk} (j, k = 1, 2, …, 6) the added mass/moment of inertia at infinite frequency (assessed based on the panel method)

K_{jk} (j, k = 1, 2, …, 6) the impulse functions (assessed based on the panel method)

C_{jk} (j, k = 1, 2, …, 6) the hydrodynamic restoring coefficients (the panel method should include the assessment)

F_j^{ex} (j = 1, 2, …, 6) the wave excitation forces (j=*1,2,3*) and moments (j=*4,5,6*) along and around *x*-, *y*- and z-axes, respectively (assessed based on the results from the panel method)

$F_{h(123)}^{pto}(t)$ and $F_{h(123)}^{spr}(t)$ are the forces from the PTOs and springs (along *x*-, *y*- and *z*-axes respectively, must be specified/calculated)

$M_{h(123)}^{pto}(t)$ and $M_{h(123)}^{spr}(t)$ are the moments from the PTOs and springs (around *x*-, *y*- and *z*-axes respectively, must be specified/calculated)

To have a complete time-domain model representation of the system, the dynamic equations of the inertial ball module are also required. These equations define the motion of the ball, primarily to determine the relative motion between the hull and the inertial ball. The resulting relative motion is then used to drive the power take-off system. The 6 DoF time-domain model and the corresponding motion equations of the inertial ball are defined in Eq. 5 below.

$$\begin{cases} m_b\ddot{x}_{b1}(t) + B_{b1}\dot{x_{b1}}(t) = F_{b1}^{pto}(t) + F_{b1}^{spr}(t) \\ m_b\ddot{x}_{b2}(t) + B_{b2}\dot{x_{b2}}(t) = F_{b2}^{pto}(t) + F_{b2}^{spr}(t)(t) \\ m_b\ddot{x}_{b3}(t) + B_{b3}\dot{x_{b3}}(t) = F_{b3}^{pto}(t) + F_{b3}^{spr}(t)(t) \\ I_{b44}\ddot{x}_{b4}(t) + B_{b4}\dot{x_{b4}}(t) = M_{b1}^{pto}(t) + M_{b1}^{spr}(t) \\ I_{b55}\ddot{x}_{b5}(t) + B_{b5}\dot{x_{b5}}(t) = M_{b2}^{pto}(t) + M_{b2}^{spr}(t) \\ I_{b66}\ddot{x}_{b6}(t) + B_{b6}\dot{x_{b6}}(t) = M_{b3}^{pto}(t) + M_{b3}^{spr}(t) \end{cases} \quad (5)$$

where m_b is the mass of the ball, I_{b44}, I_{b55}, I_{b66} are the moments of inertia of the ball. x_{bj} (where $j = 1, 2, \ldots, 6$) are defined as the motions of the ball in 6 DoF. The relevant ball motions are achieved by solving the dynamic equation.

For a sphere, the moments of inertia terms are defined as;

$$I_{b44} = I_{b55} = I_{b66} = \frac{2}{5}\, m_b R^2 \quad (6)$$

B_{bj} *(j = 1, 2,…, 6)* the linear added damping coefficient for the mass ball motions

$F_{b(1,2,3)}^{pto}$, $F_{b(1,2,3)}^{spr}$ are the forces acting on the ball from the PTOs and springs along $x-$, y– and z–axes, respectively

$M_{b(1,2,3)}^{pto}, M_{b(1,2,3)}^{spr}$ are the moments acting on the ball from the PTOs and springs around $x-$, y– and z–axes, respectively.

To enable time-domain simulations, the frequency-domain hydrodynamic coefficients obtained from the panel method are mapped into the time domain using impulse response functions (IRFs). The radiation force convolution terms are evaluated via the Cummins formulation, where the radiation impulse response functions $K_{jk}(t)$ are derived from the frequency-dependent radiation damping coefficients. The time-domain simulations are performed using a fixed integration time step of Δt=0.05 s and a total simulation duration of 3200 s, which is sufficient to ensure statistical convergence of the system response under irregular wave excitation. No additional high- or low-frequency cutoffs were applied beyond those inherent to the frequency range of the hydrodynamic data used to generate the impulse response functions.

Further details on the calculation of the connection point coordinates, as well as the translational and rotational motions of the ball, together with the related PTO force and moment formulations, are provided in the study by Sheng and Aggidis [37].

4. The Power Capture Properties and Evaluation of the Moored TALOS System models in Frequency and Time Domains

The power capture capabilities of the TALOS WEC have been studied in reported cases by Michailides et al. [31] and by Sheng and Aggidis [30]. The model settings related to different mooring configurations (i.e., soft- and hard-moored types) defined in Table 1 are used as a baseline reference. Case studies are then conducted to tune the device parameters for the selected sea state conditions. The optimized PTO settings are achieved through Genetic Algorithm (GA)-based optimization of the PTO damper parameters.

The frequency-domain model of the TALOS WEC system is evaluated using Eq. 3, and the RAOs of the motion modes for the initial system model are calculated. Fig. 3 and 4 illustrate the RAO results for the soft and hard moored configurations, respectively. In the soft-moored model (Fig. 3), the peak periods for surge, heave, and pitch motion modes are 22.4 s, 7.3 s, and 8.4 s, respectively. This shows the system's sensitivity to long-period waves, typical of the EMEC site, where the energy is often carried by swells with extended periods. The system is well-optimized for these conditions, though it may have lower efficiency in shorter-period waves. In contrast, the hard-moored model (Fig. 4) shows a reduced peak period of 8.84 s in surge mode, which is more suited to capturing energy from shorter-period waves commonly seen at EMEC. While the heave mode remains at 7.3 s, the pitch mode peak period increases to 8.8 s, indicating the system's adaptability to a broader range of wave periods.

Both mooring configurations exhibit key differences in their dynamic responses. The surge mode in the soft-moored model shows higher responses at longer periods (Tp > 10 s), which is characteristic of the soft mooring's ability to better handle long-period waves. The coupling between surge and pitch modes in both models is observed, while heave remains largely uncoupled from the other two modes. These findings indicate that the soft moored system is better suited for longer-period waves, whereas the hard-moored configuration can efficiently capture energy from a broader range of sea states, including shorter-period waves. This comparison emphasizes how the choice of mooring settings directly influences the system's performance in varying wave conditions at EMEC.

The amplitudes of the RAOs for the surge, heave, and pitch modes are not on the same scale for the soft-moored model. The surge mode exhibits significantly higher RAO amplitudes compared to the pitch and heave modes, reaching approximately 30.57 at $T_p = 22.44\ s$. This indicates that the surge mode plays a dominant role in the system's response, especially for $T_p > 7\ s$. In contrast, for the hard-moored model, the surge mode's RAO amplitude drops dramatically to around 0.03 at $T_p = 8.84\ s$, a reduction of nearly 1000 times. This substantial decrease in surge mode amplitude reduces its dominance, allowing the heave and pitch modes to contribute more significantly as active power-generating motion modes.

The heave RAO remains similar in both mooring configurations, with an amplitude of 1.18 at $T_p = 7.31\ s$. However, the pitch mode shows a shift in its peak period, from 8.4 s (with an amplitude of 0.93) in the soft-moored model to 8.8 s (with an amplitude of 0.8) in the hard-moored model. This indicates a slight variation in the resonance characteristics of the pitch mode between the two configurations.

The results clearly demonstrate that the soft-moored model is dominated by the surge mode, whereas the hard-moored model sees a significant reduction in surge mode dominance, with heave and pitch modes becoming more prominent. This highlights the importance of balancing the contributions of various motion modes to optimize the power capture potential of the TALOS WEC system.

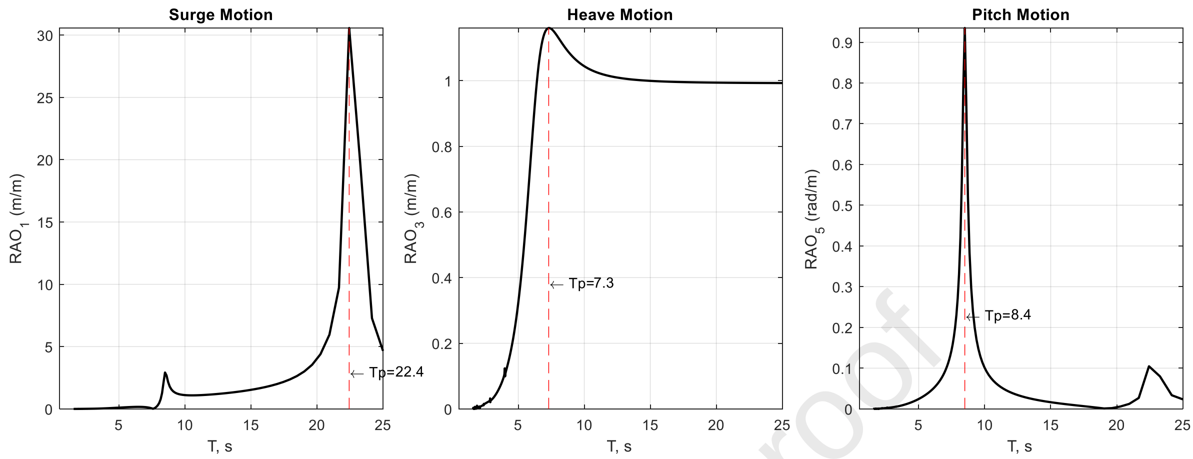

Fig. 3. Response Amplitude Operators (RAOs) of the soft moored TALOS WEC model for surge, heave, and pitch motions

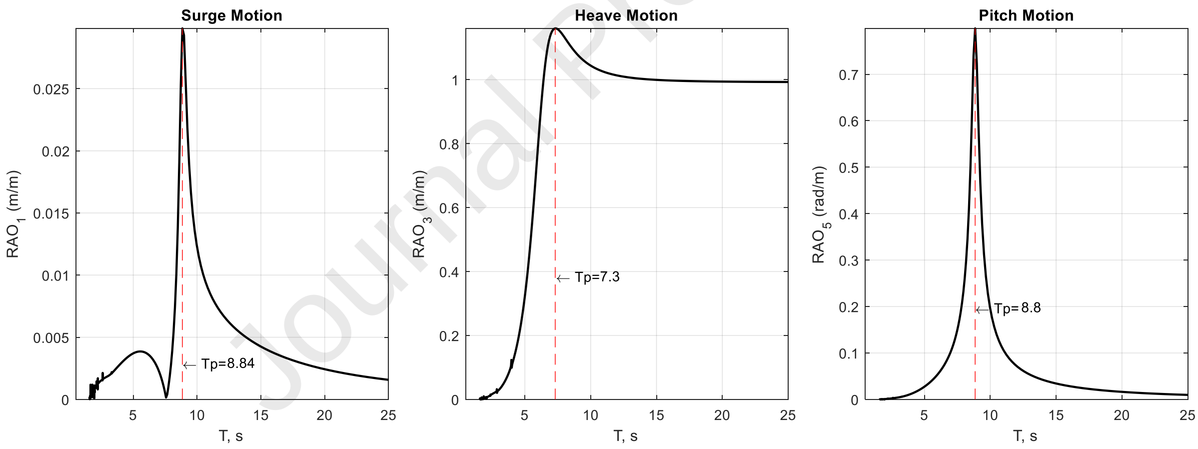

Fig. 4. Response Amplitude Operators (RAOs) of the hard moored TALOS WEC model for surge, heave, and pitch motions

The soft and hard moored TALOS system models are simulated to compare their power capture performance capabilities. For this comparison, the PTO settings are kept the same for both models, with the stiffness and damping settings of the PTO system fixed at K_{pto} = 500 kN/m and B_{pto} = 200 kNs/m, respectively.

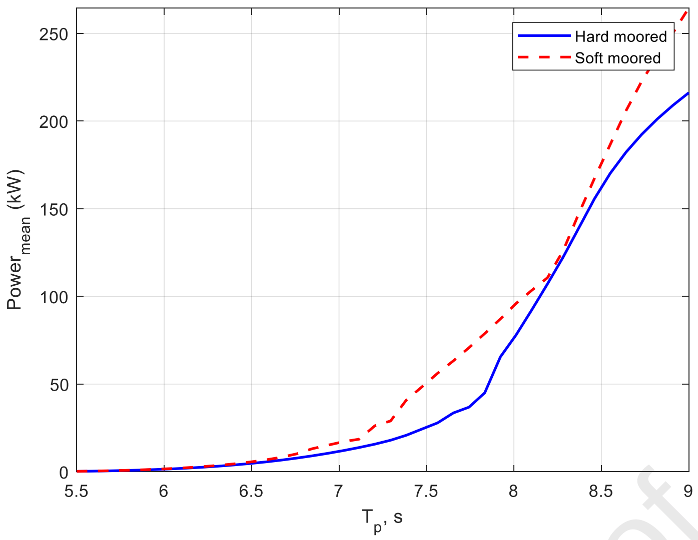

Fig. 5. Mean captured power levels for the soft-moored and hard-moored TALOS WEC models.

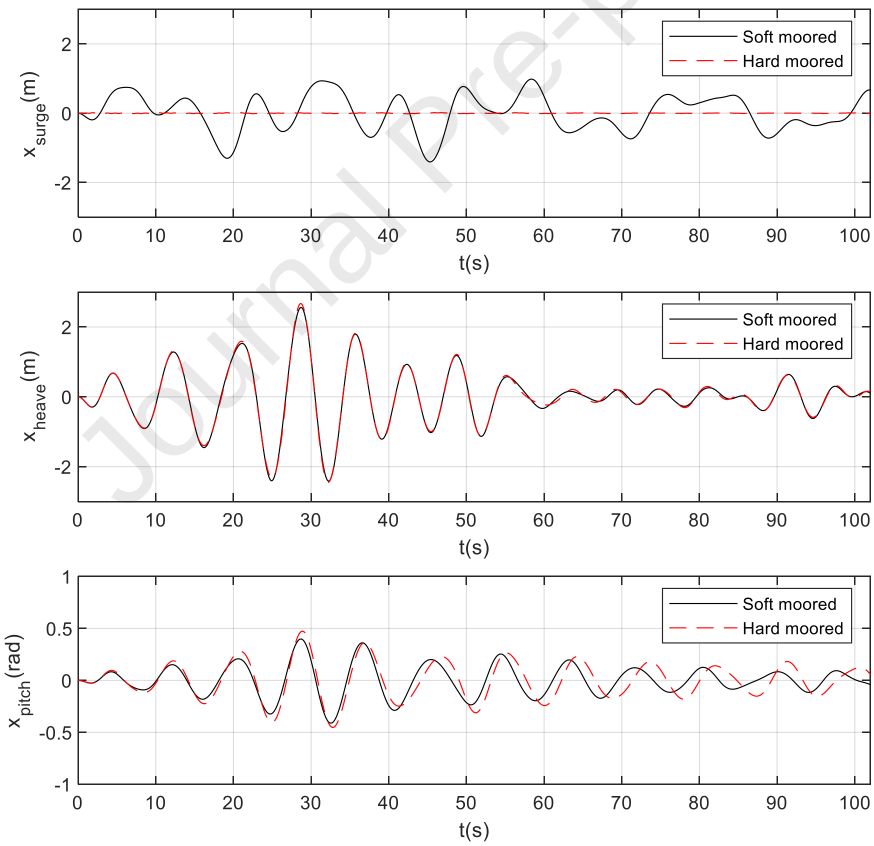

Fig. 6. Displacements of surge, heave, and pitch motion modes for the soft-moored and hard-moored TALOS WEC models.

As illustrated in Fig. 5, the soft-moored model appears to capture more power, particularly in potentially energetic sea states with $T_p > 7\ s$ (and $H_s > 2\ m$). Although the curves seem to overlap around $T_p = 8.3\ s$, the difference becomes significantly larger at $T_p = 7.75\ s$ and $T_p = 9\ s$. Fig. 6 presents the displacement results for surge, heave, and pitch motion modes in the most energetic sea state ($H_s = 4\ m$, $T_p = 9\ s$). Comparing the plots, it can be seen that due to the reduced RAO amplitude of the hard moored TALOS model, it produces very small displacements in the surge mode. On the other hand, the heave mode appears unaffected by the mooring settings, as it is not coupled with surge motion or related mooring parameters. The pitch mode displacement period shows a slight increase, with a noticeable phase difference emerging after the first half of the simulation. This shift is primarily due to the slight rightward shift in the maximum T_p value from 8.4 s to 8.8 s, as illustrated in Fig. 3 and Fig. 4.

In Fig. 7, the mooring settings and PTO damping parameters are further analyzed to clarify their combined effect on the power capture performance of the system. For this purpose, the stiffness parameter of the PTO system is set at $K_{pto} = 500\ kN/m$. The PTO damping term (B_{pto}) is varied between 50 kNs/m and 250 kNs/m, while the mooring setting (C_{11}) is varied between 500 kN/m and 8,000 kN/m. The analysis is performed for the four previously determined sea states, which correspond to the most frequent sea states for the EMEC sea site considered.

As shown in Fig. 7, the power capture levels increase with the increasing energy potential of the waves, which is a function of H_s and T_p. An important observation is the shape of the surface that defines the variation of power capture levels for varying PTO damping settings. It is evident from the figures that as the energy potential levels increase (from H_s/T_p of 1m/6s to 4m/9s waves), the plots become irregular and non-linear. In other words, optimizing with two parameters leads to the challenge of optimizing a multi-parameter, non-linear system.

It can also be seen from Fig. 7 that the optimal PTO damping term for all the sea states considered is around $B_{pto} = 200\ kNs/m$. However, there is no single surge mooring setting (C_{11}) that is suitable for all sea states. For the first sea state ($H_s = 1\ m$, $T_p = 6\ s$), the optimal surge mooring stiffness (C_{11}) is in the range of 8000 kN/m. In the second sea state ($H_s = 2\ m$, $T_p = 7\ s$), similar performance is observed for surge mooring stiffness (C_{11}) values ranging from 4000 to 8000 kN/m. For the third sea state ($H_s = 3\ m$, $T_p = 8\ s$), the power capture performance is relatively high when the surge mooring stiffness (C_{11}) is between 500 and 3000 kN/m. The results for the last sea state ($H_s = 4\ m$, $T_p = 9\ s$) show that power capture performance is significantly higher when the surge mooring stiffness (C_{11}) is in the range of 500 to 700 kN/m. It is clear that as the sea state energy potential increases, the optimal surge mooring stiffness (C_{11}) levels decrease. This is primarily because increasing surge mooring stiffness reduces the RAO period (T_p) and the RAO amplitude of the surge mode, thereby decreasing the contribution of surge motion to power capture performance. The figures clearly indicate that surge mooring stiffness plays a crucial role in the power capture performance of a WEC and should be adjusted according to the sea state conditions for optimal operation.

In Fig. 8, the power capture performance of the TALOS WEC is analyzed for surge mooring and a selected range of sea states ($0.5\ m < H_s < 5\ m$ and $5.5\ s < T_p < 10\ s$). For this analysis, the stiffness and damping settings of the PTO system are set at $K_{pto} = 500\ kN/m$ and $B_{pto} = 200\ kNs/m$, respectively. It is evident that for low-energy sea states ($0.5\ m < H_s < 1.5\ m$ and $5.5\ s$

< T_p < 6.5 s), high surge mooring stiffness (C_{11} > 6000 kN/m) increases power capture performance. However, as the energy potential of the sea state increases (2 m < H_s < 5 m and 7 s < T_p < 10 s), the suitable surge mooring settings are relatively lower (C_{11} < 2000 kN/m). To compare the performance of the TALOS WEC, two surge mooring settings (C_{11}) that meet the above criteria are defined as 1000 kN/m for low-energy sea states and 8000 kN/m for high-energy sea states. These mooring settings are used to model TALOS-L (C_{11}= 1000 kN/m) and TALOS-H (C_{11} = 8000 kN/m), corresponding to low and high surge mooring settings, respectively.

The next step is to explore the full potential of the newly defined TALOS models. To gain a clearer understanding of the results, it is essential to also optimize all PTO damping parameters $\left(B_{1,\dots,6}^{pto}\right)$ to enhance power capture performance. This optimization task becomes challenging, as the system's power capture properties are non-linear, and there are six PTO damping parameters $\left(B_{1,\dots,6}^{pto}\right)$ to consider.

The primary optimization target of this study is to maximize the mean power capture of the TALOS WEC system across different sea states by optimizing key system parameters. Specifically, the optimization focuses on determining the ideal PTO damping settings ($B_{1,\dots,6}^{pto}$) to enhance energy extraction efficiency while dynamically adapting to varying sea conditions. By addressing these optimization factors, the study aims to enhance overall system efficiency while maintaining operational stability across a range of sea states.

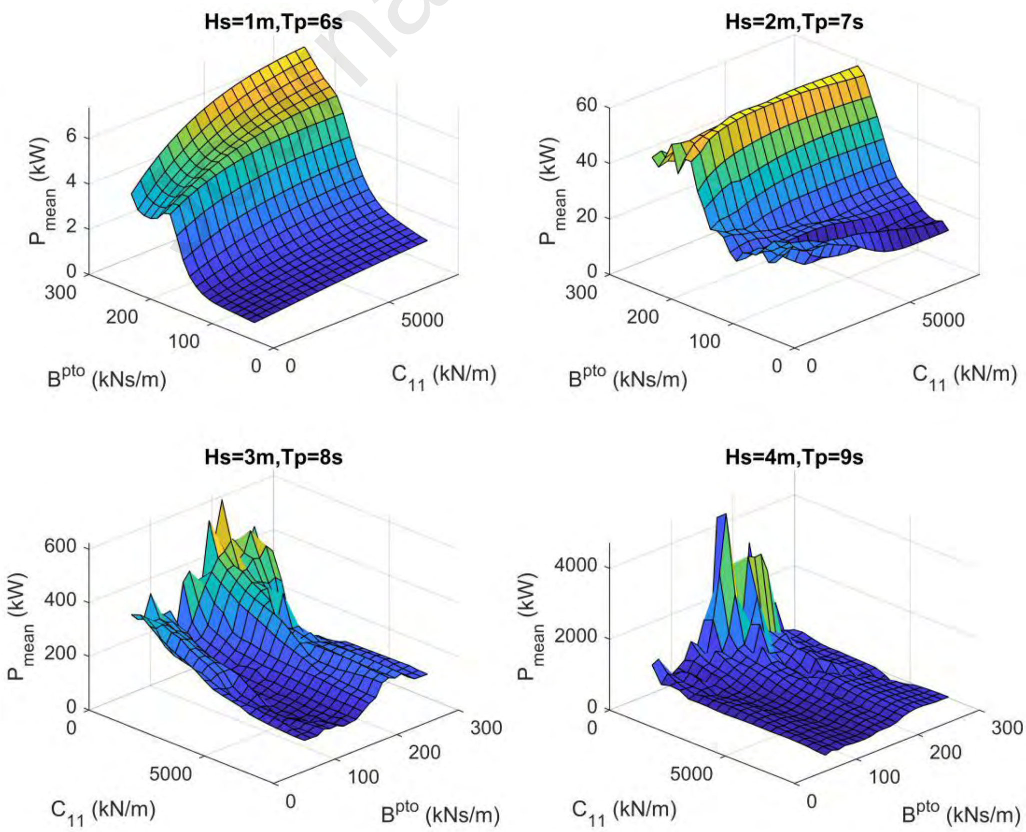

Fig. 7. Mean power capture levels for selected sea states (H_s/T_p) at varying surge mode mooring stiffness (C_{11}) and PTO damping settings (B^{pto}).

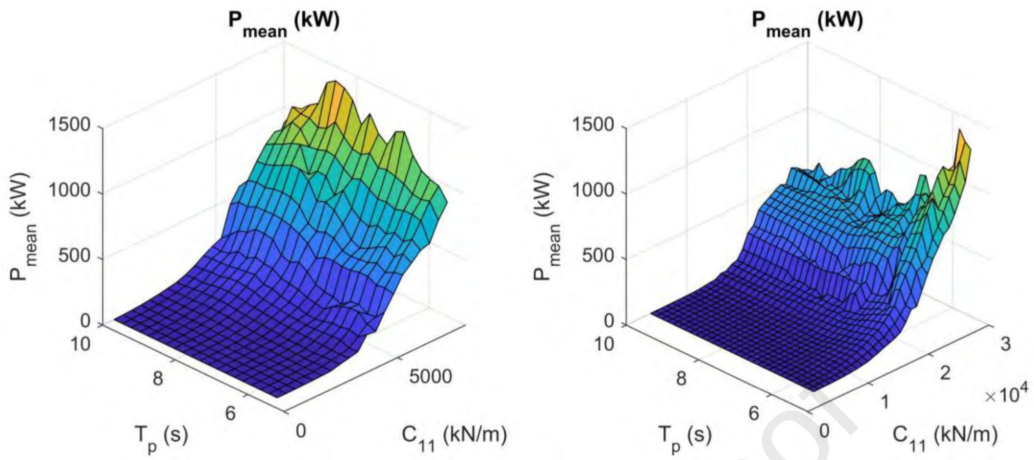

Fig. 8. Mean power capture levels for surge mode mooring stiffness (C_{11}) across sea state peak periods ($5.5\ s < T_p < 10\ s$, $0.5\ m < H_s < 5\ m$). Left: $500\ kN/m < C_{11} < 8000\ kN/m$, Right: $4000\ kN/m < C_{11} < 30000\ kN/m$.

To address the complex and multi-parameter optimization problem considered in this study, a Genetic Algorithm (GA)–based approach is adopted. Classical GA principles, including population-based search, selection, crossover, and mutation, provide a flexible framework for solving non-linear and non-convex optimization problems, as originally surveyed by Srinivas and Patnaik [38] and later formalized in standard GA methodologies by Sivanandam and Deepa [39]. More recent reviews have highlighted the robustness of GA techniques in handling discontinuous and non-differentiable objective functions, as well as their ability to maintain solution diversity and avoid premature convergence [40].

In addition, multi-objective extensions of GA have been widely recognized as effective tools for balancing competing performance metrics in complex engineering systems. Sharma and Kumar [41] emphasized the suitability of evolutionary multi-objective optimization methods for problems involving conflicting objectives, where trade-offs among system performance measures must be explicitly managed. This characteristic is particularly relevant for wave energy converter (WEC) optimization, where power capture, mechanical loading, and dynamic response constraints must be considered simultaneously.

The effectiveness of GA-based optimization in the wave energy domain has been demonstrated in several studies. Sharp and DuPont [42] applied a GA framework to optimize WEC array layouts while accounting for hydrodynamic interactions and minimum separation constraints, whereas Zeng et al. [43] employed a hierarchical GA to improve array performance under coupled hydrodynamic effects. At the device level, McCabe [44] used GA-based constrained optimization to determine optimal WEC geometry, and Shadmani et al. [45] extended this approach to the geometry design of multi-axis WEC systems. These studies collectively demonstrate that GA-based methods are well suited for the random search–based optimization of complex WEC systems with multiple design variables and competing objectives.

Although GA-based optimization can be computationally demanding and sensitive to parameter selection, these limitations are not prohibitive for the present study. The flexibility, robustness, and proven applicability of GA techniques to WEC-related optimization problems make them an appropriate choice for the multi-objective tuning task addressed here.

In the present study, the GA tool is employed to tune six PTO damping parameters ($B_{1,\dots,6}^{pto}$) simultaneously. This method enables the determination of the optimal values for all PTO system damping settings in one step. The GA optimization is performed using a 6-parameter search with a population size of 100 and 200 generations, with a constraint tolerance of 0.1. To constrain the generated PTO forces and ensure structural reliability, the upper bound for PTO damping settings is set to 3e5 with respective units for each motion mode. This constraint helps limit excessive PTO forces, reducing mechanical loads on the structure and improving reliability. Additionally, the optimization considers simultaneous tuning of all PTO damping terms for the 6-DoF system, ensuring a balanced dynamic response. By refining the system's RAOs, the approach minimizes PTO force amplitudes, leading to improved power capture efficiency while maintaining practical implementability. Simulations are conducted for both TALOS-L and TALOS-H models. The results presented in Fig. 9 provide details for the TALOS-L model in a low-energy potential sea state ($H_s = 1\ m$ and $T_p = 6\ s$). Similarly, the results presented in Fig. 10 provide details for the TALOS-H model in a high-energy potential sea state ($H_s = 3\ m$ and $T_p = 8\ s$).

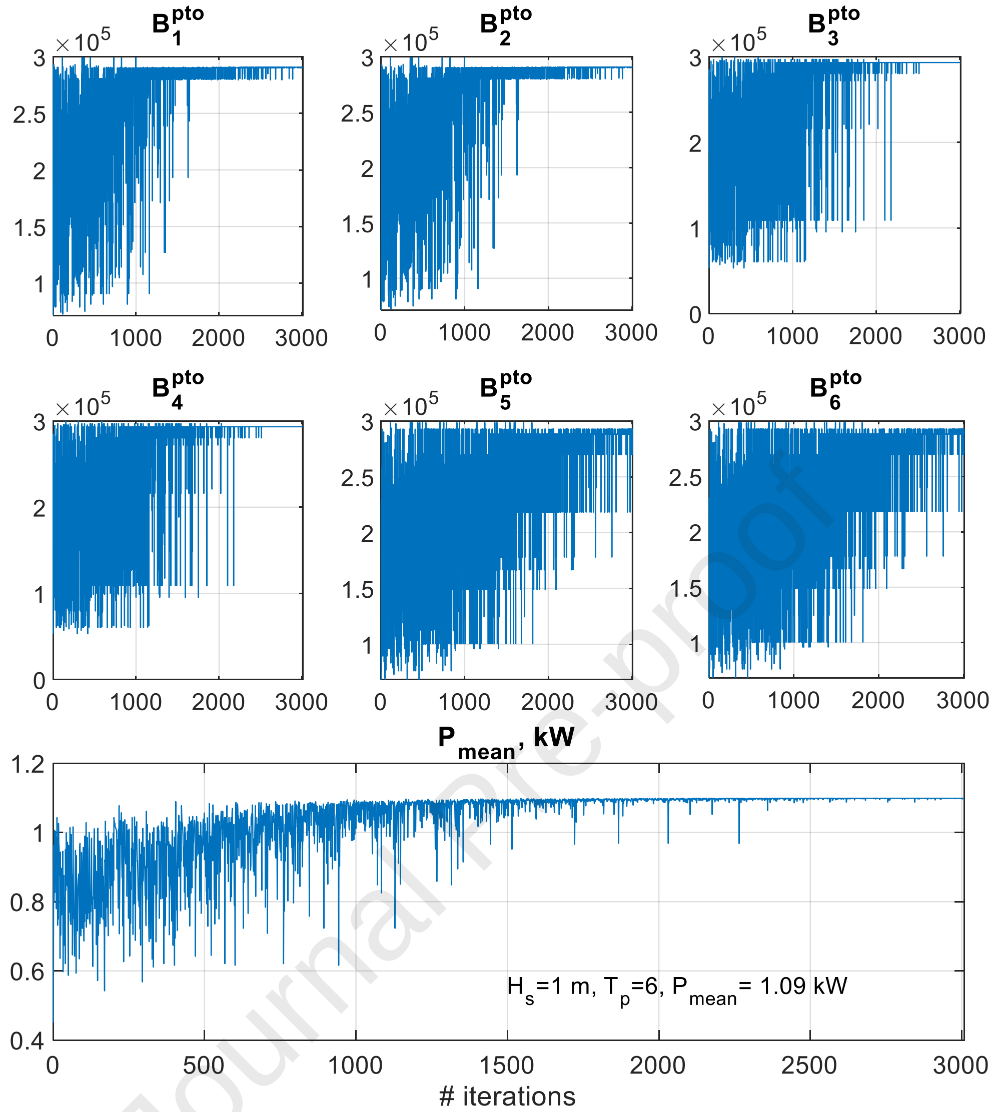

Fig. 9. Convergence of PTO damping coefficients ($B_{1,\dots,6}^{pto}$) and mean captured power (P_{mean}) for TALOS-L during GA optimization for $H_s = 1\ m$, $T_p = 6\ s$.

In Fig. 9, the TALOS-L WEC model has been optimized to tune the PTO damping settings ($B_{1,\dots,6}^{pto}$) for optimal operation in a low-energy potential sea state ($H_s = 1\ m$, $T_p = 6\ s$). The optimum PTO damping settings for all six PTO dampers are approximately 290 kNs/m, resulting in a captured power of about 1 kW. The results are based on 5000 iterations and 25 generations of the GA optimization tool, with the first 3000 iterations shown to illustrate convergence and highlight how the PTO damping terms settle toward their final values.

A similar optimization analysis is conducted for the TALOS-H WEC model. The related results are shown in Fig. 10 for a high-energy potential sea state ($H_s = 3\ m$, $T_p = 8\ s$). In this case, the optimum PTO damping settings for the six PTO dampers range from approximately 40 kNs/m to 98 kNs/m, with a captured power of about 574 kW. The results are based on 6600 iterations and 33 generations of the GA optimization tool, with the first 3200 iterations shown to illustrate convergence and highlight how each PTO damping term settles toward its final value.

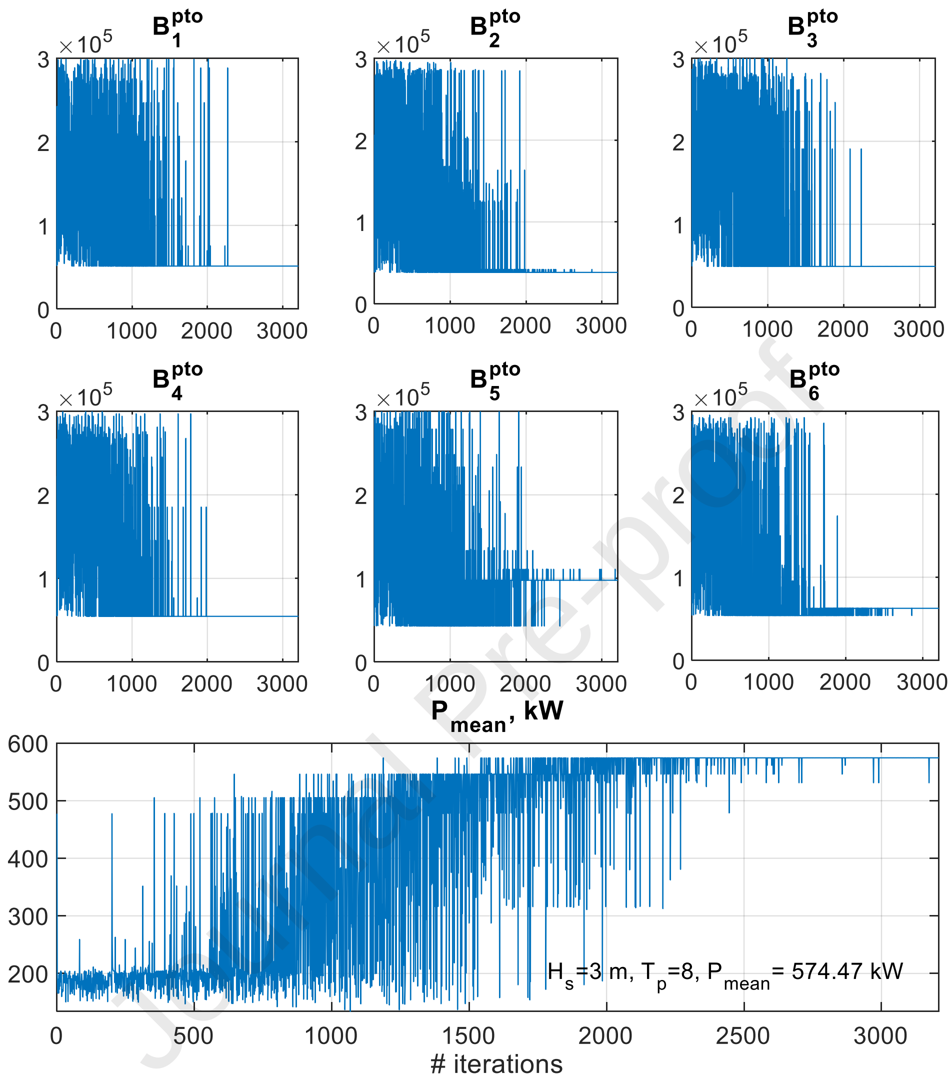

Fig. 10. Convergence of PTO damping coefficients ($B_{1,\ldots,6}^{pto}$) and mean captured power (P_{mean}) for TALOS-H during GA optimization for $H_s = 3\ m$, $T_p = 8\ s$.

In Table 3, the results of the GA-based mean power capture optimization for all selected sea states are presented. As shown in the table, the performances of the TALOS-L and TALOS-H WEC models are compared, with the details of the GA-based mean power capture optimization provided. It is also worth noting that the power capture performances of both models appear to outperform the soft and hard moored models presented by Sheng and Aggidis [30] in their study, particularly for higher-energy sea states, where the difference becomes more distinct.

Table 3. The power capture performance comparison of TALOS-L and TALOS-H models with GA tuned PTO damping parameters

Sea States (Hs/Tp)	TALOS - L				TALOS - H			
	P (kW)	B^{PTO} (k Ns/m)	Iter.	Gen.	P (kW)	B^{PTO} (k Ns/m)	Iter.	Gen.
1m / 6s	**1.09**	all about 290	5200	26	**7.48**	Ranging from 45 to 300	5200	26
2m / 7s	**27.28**	Ranging from 60 to 170	5400	27	**55.58**	Ranging from 40 to 290	7000	35
3m / 8s	**383.06**	Ranging from 53 to 75	7000	35	**574.47**	Ranging from 40 to 100	6600	33
4m / 9s	**1051.46**	Ranging from 60 to 160	8400	42	**1296.54**	Ranging from 60 to 110	8000	40

The analysis results for the TALOS WEC system models are presented. These results show that a significant amount of additional mean power can be captured for the selected sea states defined for the EMEC site. It is also worth noting that the increasing energy potential of the simulated sea states leads to a considerable increase in the captured power levels, primarily due to the selected range of mooring configurations. The defined TALOS-L and TALOS-H models appear to utilize the motion modes and benefit from multi-DoF operation, leading to an increase in power capture performance. Additionally, based on the results presented in Fig. 5, the soft-moored system outperforms the hard-moored system model. The results presented in Table 3 indicate that the TALOS-H system model performs better across all sea states due to its optimized surge mode mooring settings. It is clear that the surge mode mooring setting defined for the hard moored system, as reported by Sheng and Aggidis [30], is excessively high (250,000 kN/m), which causes a decrease in the RAO amplitude and leads to degraded device performance. The tuned version of the hard moored model (TALOS-H), with a relatively lower surge mode mooring setting (8,000 kN/m), appears to perform the best. The TALOS-H model outperforms the TALOS-L model.

Table 4. The power capture performance comparison of TALOS models for the selected sea states

	Captured power P(kw)					
(Hs/Tp)	Soft moored	Hard moored	TALOS - L	TALOS - H	Ratio (L, H)	
1m / 6s	**1.64**	**1.47**	**1.09**	**7.48**	**0.70**	**4.81**
2m / 7s	**14.59**	**11.63**	**27.28**	**55.58**	**2.08**	**4.24**
3m / 8s	**94.78**	**76.05**	**383.06**	**574.47**	**4.48**	**6.73**
4m / 9s	**264.45**	**216.14**	**1051.46**	**1296.54**	**4.38**	**5.40**

Table 4 compares the power capture performance of the TALOS WEC models in the selected sea states. The soft moored model [31] and hard moored model [30] are compared with the proposed TALOS-L and TALOS-H models. It is clear that tuning the surge mooring settings and optimizing the PTO damping settings significantly improve the performance of the TALOS WEC. The results indicate that for all sea states, TALOS-H outperforms all other models. The captured power levels are significantly higher compared to the others. The ratio term in the table represents the ratio of power captured by TALOS-L or TALOS-H to the average power of the soft moored and hard moored models. The ratio values on the left highlight the advantage of using TALOS-L, while those on the right show the advantage of using TALOS-H. It is worth noting that the TALOS-H model captures 4.81 times more power than the average of the soft moored and hard moored models for the sea state H_s/T_p = *1 m / 6 s*. For the second and fourth sea states, the ratio is approximately 4.24 and 5.40, respectively. However, the ratio peaks in the third sea state H_s/T_p = 3 m / 8 s, reaching about 6.73. In other words, the tuned and optimized TALOS-H model demonstrates exceptional performance.

5. The Power Capture Performance of the Tuned Systems models in Time Domain

In Fig. 11, the results of the time domain simulations for power capture performance are presented. The scales on the vertical axis of the plots show that as the energy density of the sea states increases, so do the captured power levels. The figures are ordered from top to bottom, starting with low energy density sea states (i.e., H_s = *1 m* to *4 m*, T_p = *6 s* to *9 s*) and progressing to higher energy densities. It can be seen from the plot that for low energy potential seas, TALOS-L and TALOS-H both capture power at nearly all instances in time, meaning the power capture performance is spread along the time axis. In the higher energy potential seas, however, there are spikes that indicate momentary high power capture relative to other instances. Another key observation is that the tuned surge mooring settings, along with the GA-based optimization of PTO damping settings, significantly enhance the system's performance. Therefore, it can be concluded that combined FD and TD GA-based optimization for the TALOS-H model results in superior performance, outperforming all other models.

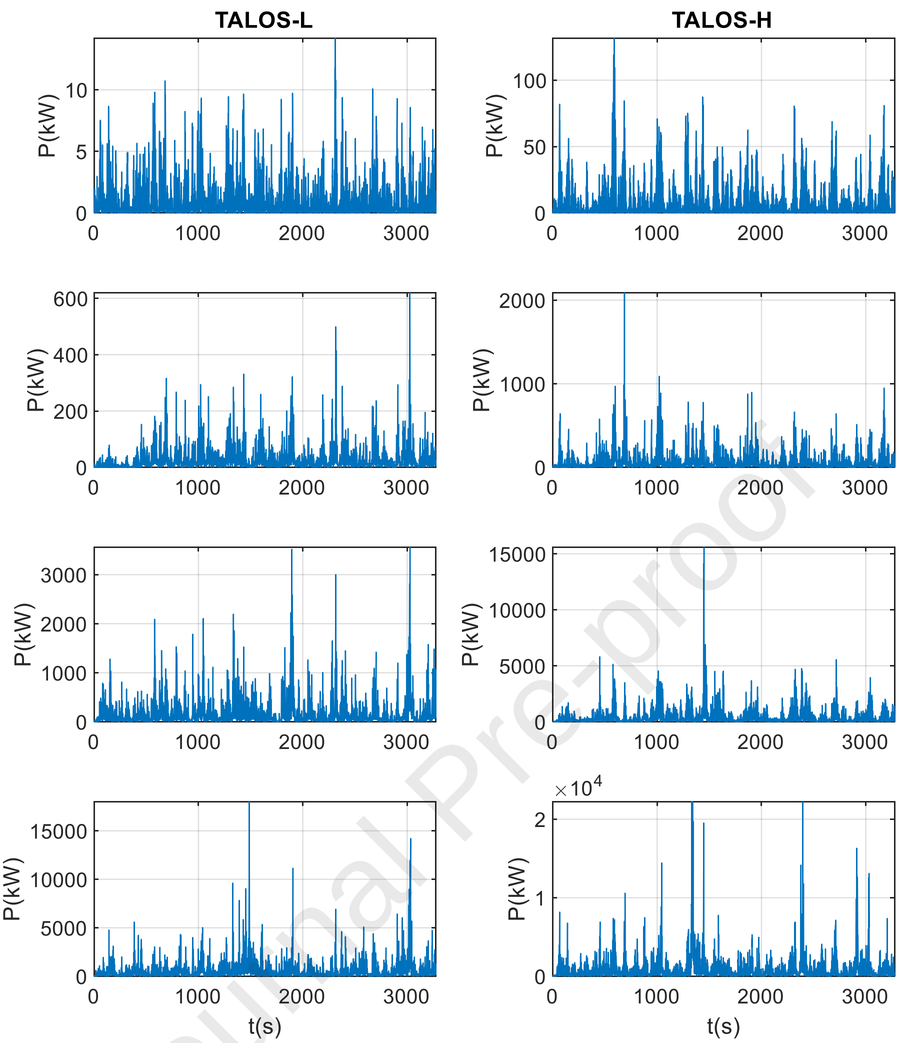

Fig. 11. Power capture plots for TALOS-L (left column) and TALOS-H (right column) across different sea states: H_s/T_p = *1m/6s, 2m/7s, 3m/8s, and 4m/9s* (ordered from top to bottom).

One of the key benefits of the proposed mooring tuning approach is the enhanced performance achieved in lower-energy potential sea states. This is particularly important because calmer sea states are common at many potential deployment sites. As a result, it is essential for the WEC device to be designed and tuned specifically for its deployment location. Therefore, evaluating the site and tailoring the device's properties accordingly is a critical consideration in the development of WEC systems.

Another important factor in site selection is the operational safety of the WEC systems under extreme sea states. Therefore, it is essential to assess the site's likelihood of experiencing such extreme conditions. Ensuring that the WEC system can reliably withstand these extreme sea states is critical for the long-term reliability and safety of the device.

The results from the simulation studies of the TALOS WEC models demonstrate a significant improvement in power capture performance compared to traditional soft and hard moored models, highlighting the contribution of the proposed system. Through the optimization of surge mooring settings and PTO damping parameters, the TALOS-L and TALOS-H models are fine-tuned to effectively capture power across a wide range of sea states, including both low and high-energy potential conditions. These results highlight the importance of device-specific tuning, as the optimized models (TALOS-L and TALOS-H) exhibited substantially higher power capture levels, particularly in higher energy sea states, compared to the soft and hard moored reference models [30, 31]. This optimization approach, supported by both frequency-domain (FD) analysis and genetic algorithm (GA)-based time-domain (TD) optimization, provides a potential solution to improving the efficiency of WEC systems. Moreover, the performance of the TALOS-H model in particular, which outperforms all other models tested, highlights the success of the tuned surge mooring settings and optimized PTO damping in enhancing the system's ability to capture power.

The contribution of this study lies not only in the proposed system's ability to capture more power but also in the methodology for tuning and optimizing the mooring and PTO settings. Unlike typical conventional systems that rely on fixed mooring settings, this study demonstrates the effectiveness of dynamic tuning based on the energy potential of the site. The findings emphasize the importance of adapting the device properties to specific site conditions, particularly for low-energy sea states, which are common at many potential deployment sites. This site-specific optimization is essential for maximizing the performance of the TALOS WEC in real-world applications. Furthermore, safety considerations for extreme sea states are incorporated into the assessment, ensuring that the TALOS WEC performs efficiently while remaining robust and reliable under adverse conditions. Thus, the results of the simulation study highlight the contribution of the proposed approach by providing clear evidence of how the optimization process enhances the overall performance and adaptability of the TALOS WEC system. The findings demonstrate that tuning mooring and PTO settings leads to substantial improvements in power capture, particularly under varying sea states. This approach illustrates how the TALOS system can be effectively optimized to match the specific energy conditions of different deployment sites, ultimately improving overall system efficiency and robustness.

Conclusions

The results presented in this study highlight the significant potential of multi degree of freedom (multi DoF) wave energy converter (WEC) systems, such as the TALOS WEC, in fully realizing the energy potential of wave energy. While much of the existing literature has focused on single degree of freedom (1 DoF) systems, this study offers a detailed analysis of a multi-DoF WEC system, demonstrating the advantages of this approach. The TALOS system's physical properties and mathematical models are presented through both frequency domain (FD) and time domain (TD) analyses, with a focus on the site-specific sea state conditions of the EMEC site.

In the FD analysis, the role of mooring settings in shaping the response amplitude operators (RAOs) of the motion modes is examined. Two new models, TALOS-L and TALOS-H, are proposed based on these analyses, revealing that mooring settings have a considerable impact on surge mode RAOs, while pitch and heave modes are less affected. Additionally, the study emphasizes the importance of PTO damping settings in optimizing power capture performance, showing that the optimum PTO damping value for all sea states considered is around 200 kNs/m. For instance, TALOS-L under low-energy sea state conditions ($H_s=1$ *m*, $T_p=6$ *s*) captures 1 kW of power, while TALOS-H under high-energy conditions ($H_s=3$ *m*, $T_p=8$ *s*) reaches a power capture of 574 kW.

A key contribution of this study is the use of Genetic Algorithm (GA) optimization to fine-tune the PTO damping settings. This analysis shows that GA-based optimization enables the simultaneous determination of optimal damping values, highlighting the need for sea state-specific adjustments to achieve high performance. The study demonstrates that, in general, PTO damping settings should be higher for lower-energy sea states and lower for higher-energy sea states.

The findings underline the importance of adapting the WEC system to the specific conditions of the deployment site. By optimizing the mooring settings to match the RAOs of the motion modes with site conditions, the TALOS system is able to significantly increase its power capture potential. Particularly, the TALOS-H model demonstrates superior performance across all considered sea states, suggesting that it can generate substantially more power than other models. This study also emphasizes the critical role of tuning the PTO system for site-specific conditions, and the use of AI tools such as GA for optimizing the system's performance.

Overall, the study demonstrates that the TALOS WEC system's power capture capabilities can be significantly enhanced by customizing its settings to suit the energy characteristics of the deployment site. The results, with specific improvements in power levels and through optimization of PTO damping, reinforce the potential of the proposed approach, showing that a combination of mooring tuning, PTO damping optimization, and AI-based techniques can lead to improved performance across a range of sea states.

The proposed approach enables the WEC system to be tailored to the energetic wave conditions of a specific sea site. By optimizing the system’s dynamic response, it minimizes the range of PTO forces required to adapt to varying sea states. As a result, this method not only enhances power capture performance but also reduces PTO force amplitudes, contributing to improved reliability and overall operational efficiency of the WEC.

Future research can focus on integrating advanced control strategies, incorporating structural and cost constraints in optimization, and validating findings through experimental testing. Further studies can also explore multi-WEC array interactions, alternative PTO mechanisms, and multi-objective optimization approaches for improved efficiency and reliability. Additionally, assessing the system’s performance under extreme sea states will enhance its long-term survivability.

CRediT authorship contribution statement

Hakan Yavuz: Conceptualization, formal analysis, funding acquisition, project administration, funding acquisition, methodology, writing, editing, – original draft. **Wanan Sheng:** Investigation, review & editing, conceptualization. **George Aggidis:** Funding acquisition, project administration, review & editing.

Declaration of competing interest

The authors declare the following financial interests/personal relationships which may be considered as potential competing interests:

Hakan Yavuz reports financial support was provided by TUBITAK, TURKIYE. George Aggidis reports financial support was provided by Engineering and Physical Sciences Research Council.

Acknowledgments

This work was partly supported by the UK Engineering and Physical Sciences Research Council (EPSRC grant number EP/V040561/1: "NHP-WEC") for the TALOS WEC project. The hydrodynamic analysis and initial developments of TALOS wave energy converter system model are performed as a part the EPSRC supported project.

The study was also partly supported by TUBITAK (Grant Number: 124M015). As a part of the TUBITAK supported project, the Frequency Domain and Time Domain analysis studies as well as Genetic Algorithm based optimization studies are performed for improved power capture performance.

References

[1] C.V.C. Weiss, R. Guanche, B. Ondiviela, O.F. Castellanos, J. Juanes, Marine renewable energy potential: A global perspective for offshore wind and wave exploitation, Energy Conversion and Management 177 (2018) 43-54. https://doi.org/10.1016/j.enconman.2018.09.059

[2] Z. Shao, H. Gao, B. Liang, D. Lee, Potential, trend and economic assessments of global wave power, Renewable Energy 195 (2022) 1087-1102. https://doi.org/10.1016/j.renene.2022.06.100

[3] B. Robertson, 8.02 - Wave Energy: Resources and Technologies, Comprehensive Renewable Energy (2nd Ed.) 8 (2022) 10-24, Editor(s): Trevor M. Letcher, Elsevier, ISBN: 9780128197349.

[4] T.W. Thorpe, A brief review of wave energy, *ETSU Report* Number R-120 for the DTI (1999). http://large.stanford.edu/courses/2012/ph240/thomas2/docs/ ETSU-R120.pdf

[5] G. Mørk, S. Barstow, A. Kabuth, M.T. Pontes, Assessing the global wave energy potential, Proceedings of the ASME 2010 29th International Conference on Ocean, Offshore and Arctic Engineering, OMAE2010 - 20473, (2010) Shanghai, China. https://doi.org/10.1115/OMAE2010-20473

[6] I. Iancu, A.W. Clarke, J.A. Trinnaman, World Energy Council, Wave energy, The 2010 Survey of Energy (Chapter 14) (2010), ISBN: 978 0 946121 021. (https://www.worldenergy.org/ assets/ downloads/ser_2010_report_1.pdf)

[7] H. Yavuz, S. Mistikoglu, T. Thorpe, G. Aggidis, T. Stallard, Chapter 16 - Wave Energy: Available Technologies and R&D Status, Energy Science and Technology, Vol.9, Geothermal and Ocean Energy, (2015) 420-453.

[8] H. Eidsmoen, Tight-moored amplitude-limited heaving-buoy wave-energy with phase control, Applied Ocean Research 20 (1998) 157–61. https://doi.org/10.1016/S0141-1187(98)00013-3

[9] U. A. Korde, On providing a reaction for efficient wave energy absorption by floating devices, Applied Ocean Research 21 (1999) 235–48. https://doi.org/10.1016/S0141-1187(99)00009-7

[10] U. A. Korde, Latching control of deep water wave energy devices using an active reference, Ocean Engineering 29 (2002) 1343–55. https://doi.org/10.1016/S0029-8018(01)00093-2

[11] U. A. Korde, Systems of reactively loaded coupled oscillating bodies in wave energy conversion, Applied Ocean Research 25 (2003) 79–91. https://doi.org/10.1016/S0141-1187(03)00044-0

[12] A. Babarit, G. Duclos, A. H. Clement, Comparison of latching control strategies for a heaving wave energy device in random sea, Applied Ocean Research 26 (2004) 227–38. https://doi.org/10.1016/j.apor.2005.05.003

[13] G. Nolan, M. O. Cathai, J. Murtagh, J. V. Ringwood, Modelling and simulation of the power take-off system for a hinge-barge wave energy converter, *Fifth European Wave Energy Conference*, University of Cork, Ireland, September, (2003) 38–45. https://mural.maynoothuniversity.ie/id/ eprint/4424/

[14] T. Bjarte-Larsson, J. Falnes, Laboratory experiment on heaving body with hydraulic power take-off and latching control, Ocean Engineering 33 (2006) 847–877. https://doi.org/10.1016/j.oceaneng.2005. 07.007

[15] H. Shi, F. Cao, Z. Liu, N. Qu, Theoretical study on the power take-off estimation of heaving buoy wave energy converter, Renewable Energy, 86 (2016) 441-448. https://doi.org/10.1016/j.renene.2015.08.027

[16] M. Shadman, S.F. Estefen, C.A. Rodriguez, I.C.M. Nogueira, A geometrical optimization method applied to a heaving point absorber wave energy converter, Renewable Energy, 115 (2018) 533-546. https://doi.org/10.1016/j.renene.2017.08.055

[17] J. Tan, H. Polinder, A.J. Laguna, S. Miedema, The application of the spectral domain modeling to the power take-off sizing of heaving wave energy converters, Applied Ocean Research, 122 (2022) 103110. https://doi.org/10.1016/j.apor.2022.103110

[18] H. Liang, D. Qiao, X. Wang, G. Zhi, J. Yan, D. Ning, J. Ou, Energy capture optimization of heave oscillating buoy wave energy converter based on model predictive control, Ocean Engineering, 268 (2023) 113402. https://doi.org/10.1016/j.oceaneng.2022.113402

[19] N.H.D.S. Manawadu, I.D. Nissanka, H.C.P. Karunasena, SPH-based numerical modelling and performance analysis of a heaving point absorber type wave energy converter with a novel buoy geometry, Renewable Energy, 228 (2024) 120595. https://doi.org/10.1016/j.renene.2024.120595

[20] A.J. Hillis, C. Whitlam, A. Brask, J. Chapman, A.R. Plummer, Active control for multi-degree-of-freedom wave energy converters with load limiting, Renewable Energy 159 (2020), 1177-1187. https://doi.org/10.1016/j.renene.2020.05.073

[21] H. Yavuz, On Control of a Pitching and Surging Wave Energy Converter, International Journal of Green Energy, 8:5 (2011) 555-584. https://doi.org/10.1080/15435075.2011.576291

[22] O. Abdelkhalik, S. Zou, R.D. Robinett, G. Bacelli, D.G. Wilson, R. Coe, U. Korde, Multiresonant feedback control of a three-degree-of-freedom wave energy converter, IEEE Trans. Sustain. Energy 8 (4) (Oct 2017) 1518-1527. https://doi.org/10.1109/TSTE.2017.2692647

[23] D.E. Galvan-Pozos, F.J. Ocampo-Torres, Dynamic analysis of a six-degree of freedom wave energy converter based on the concept o f the Stewart-Gough platform, Renewable Energy 146 (2020) 1051-1061. https://doi.org/10.1016/j.renene.2019.06.177

[24] D.V. Evans, D.C. Jeffrey, S.H. Salter, J.R.M. Taylor, Submerged cylinder wave energy device: theory and experiment, Appl. Ocean Res. 1 (1) (1979) 3-12. https://doi.org/10.1016/0141-1187(79)90003-8

[25] S.S. Ngu, D.G. Dorrell, E. Acha, Control of a Bristol cylinder for wave energy generation, in: The 2010 International Power Lectronics Conference - ECCE ASIA, June 2010, pp. 3196-3203. https://doi.org/10.1109/IPEC.2010.5542006

[26] S. Crowley, R. Porter, D.V. Evans, A submerged cylinder wave energy converter, J. Fluid Mech. 716 (2013) 566-596. https://doi.org/10.1017/jfm.2012.557

[27] G.A. Aggidis, C.J. Taylor, Overview of wave energy converter devices and the development of a new multi-axis laboratory prototype, IFAC-PapersOnLine, 50(1) (2017) 15651-15656. https://doi.org/10.1016/j.ifacol.2017.08.2391

[28] Sheng, E. Tapoglou, X. Ma, C.J. Taylor, R.M. Dorrell, D.R. Parsons, G. Aggidis, Hydrodynamic studies of floating structures: Comparison of wave-structure interaction modelling, Ocean Engineering, 249 (2022) 110878. https://doi.org/10.1016/j.oceaneng.2022.110878

[29] C. Hall, W. Sheng, Y. Wu, G. Aggidis, The impact of model predictive control structures and constraints on a wave energy converter with hydraulic power take off system, Renewable Energy, 224 (2024) 120172. https://doi.org/10.1016/j.renene.2024.120172

[30] W. Sheng, G. Aggidis, Hydrodynamic comparisons of TALOS wave energy converter using panel methods, Proc. of the 33rd Int. Ocean and Polar Eng. Conf, Ottawa, Canada, June 19-23, (2023) 597-604.

[31] C. Michailides, E. Loukogeorgaki, W. Sheng, G. Aggidis, Time-domain analysis of the TALOS wave energy converter using different computational tools, Proc. of the 33rd Int. Ocean and Polar Eng. Conf, Ottawa, Canada, June 19-23, (2023) 605-612.

[32] H. Yavuz, G. Aggidis, W. Sheng, An Initial Study on Power Capture Performance Analysis of TALOS Based on Power Take-Off System Parameters, Proc. of the 33rd Int. Ocean and Polar Eng. Conf, Ottawa, Canada, June 19-23, (2023) 590-596.

[33] WAMIT, User Manual (v73). https://www.wamit.com/manualupdate/ v73_manual.pdf (cited on: 01/11/2021).

[34] A. Babarit, J. Hals, M.J. Muliawan, A. Kurniawan, T. Moan, J. Krokstad, Numerical benchmarking study of a selection of wave energ y converters, Renewable Energy 41 (2012) 44-63. https://doi.org/10.1016/j.renene.2011.10.002

[35] W. F. Cummins, The Impulse Response Function and Ship Motions, Schiffstechnik 1962; 9(47):101-109. http://hdl.handle.net/1721.3/49049

[36] H.N. Nguyen, P. Tona, Short-term wave force prediction for wave energy converter control, Control Engineering Practice 75 (2018) 26-37, https://doi.org/10.1016/j.conengprac.2018.03.007.

[37] W. Sheng, G. Aggidis. Optimizations for improving energy absorption of TALOS WEC, Proc. of the 34rd Int. Ocean and Polar Eng. Conf, Rhodes, Greece, June 17-21, (2024), 608-615.

[38] M. Srinivas and L. M. Patnaik, Genetic algorithms: a survey, Computer 1994; 27(6):17-26. https://doi.org/10.1109/2.294849 .

[39] S. N. Sivanandam, S. N. Deepa, (2008). "Genetic Algorithms." In: Introduction to Genetic Algorithms. Springer, Berlin, Heidelberg.

[40] S. Katoch, S.S. Chauhan, V. Kumar, A review on genetic algorithm: past, present, and future. Multimed Tools Appl 2021; 80:8091–8126. https://doi.org/10.1007/s11042-020-10139-6

[41] S. Sharma, V. A Kumar, Comprehensive Review on Multi-objective Optimization Techniques: Past, Present and Future. Arch Computat Methods Eng 2022; 29:5605–5633. https://doi.org/10.1007/s11831-022-09778-9

[42] C. Sharp, B. DuPont, Wave energy converter array optimization: A genetic algorithm approach and minimum separation distance study, Ocean Engineering 163, (2018), 148-156. https://doi.org/10.1016/j.oceaneng.2018.05.071

[43] X. Zeng, Q. Wang, Yuanshun Kang, Fajun Yu, Hydrodynamic interactions among wave energy converter array and a hierarchical genetic algorithm for layout optimization, Ocean Engineering, 256, (2022), 111521. https://doi.org/10.1016/j.oceaneng.2022.111521

[44] A.P. McCabe, Constrained optimization of the shape of a wave energy collector by genetic algorithm, Renewable Energy, 51, (2013), 274-284. https://doi.org/10.1016/j.renene.2012.09.054

[45] A. Shadmani, M.R. Nikoo, A.H. Gandomi, M. Chen, An optimization approach for geometry design of multi-axis wave energy converter, Energy, 301, (2024), 131714. https://doi.org/10.1016/j.energy.2024.131714

Declaration of interests

☐ The authors declare that they have no known competing financial interests or personal relationships that could have appeared to influence the work reported in this paper.

☒ The authors declare the following financial interests/personal relationships which may be considered as potential competing interests:

Hakan YAVUZ reports financial support was provided by TUBITAK. George AGGIDIS reports a relationship with Engineering and Physical Sciences Research Council that includes: funding grants. If there are other authors, they declare that they have no known competing financial interests or personal relationships that could have appeared to influence the work reported in this paper.